Open Access Full Text Article

ORIGINAL RESEARCH

PAI/MRI Visualization of Tumor Derived Cellular Microvesicles with Endogenous Biopolymer Nanoparticles Modification

Shuxin Lv*, Jinghua Sun*, Chunyan Guo [ID], Yufei Qin, Ruiping Zhang

The Third Hospital of Shanxi Medical University, Shanxi Bethune Hospital, Shanxi Academy of Medical Sciences, Taiyuan, 030032, People's Republic of China

*These authors contributed equally to this work

Correspondence: Ruiping Zhang, Email zrp_7142@sxmu.edu.cn

Background: Tumor derived cellular microvesicles (TDMVs), as excellent drug delivery vehicles in vivo, play an important role in the treatment of cancers. However, it is difficult to obtain intuitional biodistribution behavior and internalization mechanisms of TDMVs in vivo. Thus, it is very urgent and important to establish a stable and reliable visualization technology to track the biological behavior and function of TDMVs. As an endogenous biopolymer, melanin possesses natural biocompatibility and biodegradability, and various biological imaging could be realized by modifying it. Therefore, melanin-based nanoparticles are excellent candidates for in vivo visualization of TDMVs.

Methods: In this work, the biodistribution and metabolic behavior of TDMVs were visualized by dual-modality imaging with PAI and MRI after incubation with gadolinium ion-chelated melanin nanoparticles.

Results: In this study, MRI and PAI dual-modality imaging of the in vivo distribution behavior of TDMVs was achieved with the help of MNP-Gd. The good targeting ability of TDMVs at the homologous tumor site was observed, and their distribution and metabolism behavior in the whole body were studied at the meantime. The results indicated that TDMVs preferentially accumulated in syngeneic tumor sites and liver regions after intravenous injection and were eventually metabolized by the kidneys over time.

Conclusion: This work proposed a novel dual-modal imaging strategy for the visualization of TDMVs, which is of great significance for further understanding the biological mechanisms of extracellular vesicles.

Keywords: cellular microvesicles, magnetic resonance imaging, photoacoustic imaging, melanin nanoparticles

Introduction

Cellular microvesicles (MVs) are vesicular structures surrounded by lipid bilayers that shed from cells in response to various stimuli, and acquire membrane components and phagocytosed cytoplasmic contents from these cells.[1] According to their biogenesis, extracellular vesicles are classified to exosomes, microvesicles, and apoptotic bodies. Both exosomes and extracellular vesicles are cell-derived vesicles ranging in diameters from 30 nm to 2000 nm.[2,3] Cell-derived vesicles own good biocompatibility and could pass through various biological barriers, thereby playing an essential role in intercellular communication.[4–6] In addition, MVs are considered as ideal drug carriers and thus are widely used in nano-drug delivery projects.[7–10]

In particular, tumor cell-derived MVs (TDMVs) possess good biocompatibility and unique surface protein expression derived from their parental cells, making them an excellent drug delivery vehicle.[11–18] However, the mechanism by which TDMVs function in the body is still unclear.[19] Understanding cargo transport and delivery of TDMVs in vivo is one of the main challenges hindering successful implementations of future TDMVs derived platforms.[20,21] Additionally, the precise knowledge of the location of TDMVs in vivo is key to understanding the precise cargo transport and internalization mechanisms. Therefore, it is necessary to utilize imaging tracking technology to realize the visualization of TDMVs.[22–24]

With the rapid development of nanotechnology and molecular imaging, engineering nanoparticles are expected to be potential candidates for visualizing the localization and functional behavior of TDMVs.[25]

Among all non-invasive molecular and functional imaging techniques, magnetic resonance imaging (MRI) has been widely used in the biomedical field as a non-invasive technique with the advantages of high spatiotemporal resolution and good soft tissue contrast.[26,27] Contrast agents could enhance the relaxation of protons in water, which is of great significance for continuously improving the MRI contrast of different tissues and organs and achieving accurate detection of diseases.[28] In particular, gadolinium (Gd)-based contrast agents have attracted substantial attention as T1-weighted MRI contrast agents and have been widely used in clinical practice.[29] In addition to traditional MRI, photoacoustic imaging (PA), as a rapidly evolving imaging technology, has great application potential in biomedical field due to its high contrast and high spatial resolution.[30] At the same time, the development of nanotechnology has made a significant contribution to the development of nanoparticle-based contrast agents for PA imaging.

Compared with exogenous materials, melanin, as an endogenous biomaterial, has excellent biosafety in vivo due to its native biocompatibility and biodegradability.[31] Moreover, melanin nanoparticles have many potential applications in biomedicine due to their properties including metal ion chelation and strong optical absorption in the near-infrared region.[32–39] Herein, water-soluble Gd-based melanin nanoparticles (MNP-Gd) have been constructed as an MRI/PAI dual-modal imaging contrast agent by a facile route. After modifying the TDMVs with the nanoparticles, the visualization of their biological distribution behavior is realized, which is of great significance for understanding the positioning distribution and metabolism of TDMVs in the body.

Materials and Methods
Synthesis of MNP-Gd
MNP-Gd was obtained according to a previously published method with some modifications.[40] After modifying melanin with polyethylene glycol, 0.6 mL of $GdCl_3$ solution (10 mg/mL) was added to 1 mL PEGylatated MNP solution (2 mg/mL) and stirred for 2 h at room temperature. The final products were centrifuged and washed 4 times with DI water to obtain the final MNP-Gd.

Characterization
UV-Vis-NIR absorption spectra were recorded at room temperature with UV-Vis-NIR spectrometer (lambda-950, Perkin Elmer). Transmission electron microscopy (TEM) of TDMVs and TDMVs+MNP-Gd were measured using a JEM-2100F microscope. The hydrodynamic diameter and zeta potential of the TDMVs, MNP-Gd and TDMVs+MNP-Gd were performed using a Nano-Zetasizer (Malvern Instruments Ltd).

Generation and Isolation of TDMVs
Murine hepatocarcinoma cell line H22 were purchased from Beyotime Biotechnology (Shanghai) Co., Ltd., and cultured according to the guidelines given. The H22 cells were cultured in DMEM medium containing 10% fetal bovine serum (FBS) at 37°C under 5% CO_2. Then the H22 cells were irradiated with ultraviolet light for 1 h to further apoptosis induction. After 12 h, supernatants were first centrifuged for 8 min at 1300 g to get rid of cells and then centrifuged for 2 min at 14,000 g to remove debris. At last, the supernatant was further centrifuged for 60 min at 14,000 g to pellet TDMVs. The pellets were washed three times and resuspended in culture medium for the following experiments.

Preparation of TDMVs+MNP-Gd
MNP-Gd and TDMVs were incubated overnight at the ratio of 1:1 in a 4°C environment. The pellets obtained after centrifugation of the mixture were washed three times and resuspended in PBS to obtain the final TDMVs+MNP-Gd products.

In vitro PAI and MRI Study

For PA imaging in vitro, a phantom filled with TDMVs+MNP-Gd in different concentrations of MNP (25, 50, 100, 200, and 400 μg/mL) was measured using a real-time multispectral optoacoustic tomographic (MSOT) imaging system (inVision 128, iThera Medical GmbH, Neuherberg, Germany). Finally, the PA signals of each sample were measured in regions of interest (ROIs), and the correlation between the PA signal and concentration curve was calculated.

To evaluate the magnetic resonance (MR) contrast enhancement effect, 200 μL of TDMVs+MNP-Gd with various concentrations of Gd^{3+} (0.05, 0.1, 0.2, 0.4, and 0.6 mM) were imaged by using a clinical 3.0 T MR clinical scanner (Magnetom Trivo with Tim, Siemens, Germany). The r_1 values were calculated from the slope of the curve-fitting result of 1/T1 (s^{-1}) versus Gd component concentration (mM).

In vivo PAI and MRI Study

All animal procedures were performed in accordance with the Guidelines for Institutional Animal Care and Use Committee and approved by the Animal Ethics Committee of Shanxi Medical University (No. SYDL2019002). Mouse hepatocarcinoma tumor H22 cells (1×10^6) suspended in 50 μL PBS were subcutaneously implanted on the dorsum region of the right leg to generate a subcutaneous H22 tumor model.

For in vivo PA imaging, H22 tumor-bearing nude mice (n=3) were intravenously injected with 200 μL TDMVs +MNP-Gd solution (3 mg/mL) via the tail vein. After injection, the images of tumor regions were collected at pre-injection, 30 min, 2 h, 4 h, 6 h, 8 h, 12 h, and 24 h post-injection. Besides, the MRI images of tumor sites at different points were also collected.

Analyses of Biodistribution

Mice were intravenously injected with TDMVs+MNP-Gd (3 mg/mL) (n=3). The images of the main organs were collected at 15 min, 4 h, 6 h, 8 h, 12 h, and 24 h post-injection. Besides, the PA signal intensities of the different sites at different points were also quantitatively analyzed. The amount of gadolinium ions in the organs was analyzed by ICP-MS to further analyze the biodistribution behavior of TDMVs (Agilent 7500 CE, Agilent Technologies, Waldbronn, Germany).

Results and Discussion

TDMVs with particle sizes in the range of 100–1000 nm were obtained by differential centrifugation. To elucidate the mechanism of biodistribution and metabolism of TDMVs, MNP-Gd was co-incubated with it and then centrifuged to obtain black precipitate products. The UV-Vis-NIR spectrum was applied to confirm that the MNP-Gd had been attached to TDMVs. There were no characteristic peaks in the TDMVs group shown in the UV-Vis-NIR spectrum, while the MNP-Gd and TDMVs+MNP-Gd groups exhibited similar broad good absorbance performance from 680 nm to 980 nm, indicating that they had been successfully combined and could be further used as potential contrast agents for PAI (Figure 1A). Dynamic light scattering (DLS) and transmission electron microscopy (TEM) analysis showed that TDMVs +MNP-Gd had a diameter about 159.4 nm, which was similar with TDMVs (Figure 1B and D). Moreover, the TEM image showed that the color of TDMVs modified with MNP-Gd turned black compared with pure TDMVs. The zeta potentials of pure TDMVs and MNP-Gd were −23.5 mV and 1.8 mV respectively, and the potential of TDMVs+MNP-Gd was −21.7 mV, further confirming that TDMVs were successfully labeled by MNPs. (Figure 1C). By evaluating the particle size changes of TDMVs+MNP-Gd in PBS and culture media after 24 h and 48 h incubation, TDMVs+MNP-Gd was found to have good stability in the physiological environment, which further verified that it could function as a stable in vivo tracer for TDMVs (Figure S1). To measure the cytotoxicity profiles of MNP-Gd, MTT (3-(4,5-dimethylthiazol-2-yl)-2,5-diphenyltetrazolium bromide) assay was carried out on murine hepatocarcinoma H22 cells and healthy Chinese hamster ovary (CHO) cells. It was found that the MNP-Gd had no obvious toxicity to H22 cells and CHO cells even at a high concentration of 800 μg/mL, which may be attributed to the native biocompatibility of melanin nanoparticles (Figure S2).

The melanin nanoparticles were proved to be an excellent PAI contrast agent in previous work.[38] The PAI signals of TDMVs+MNP-Gd were monitored to evaluate their photoacoustic properties in vitro. The PA images of TDMVs+MNP-
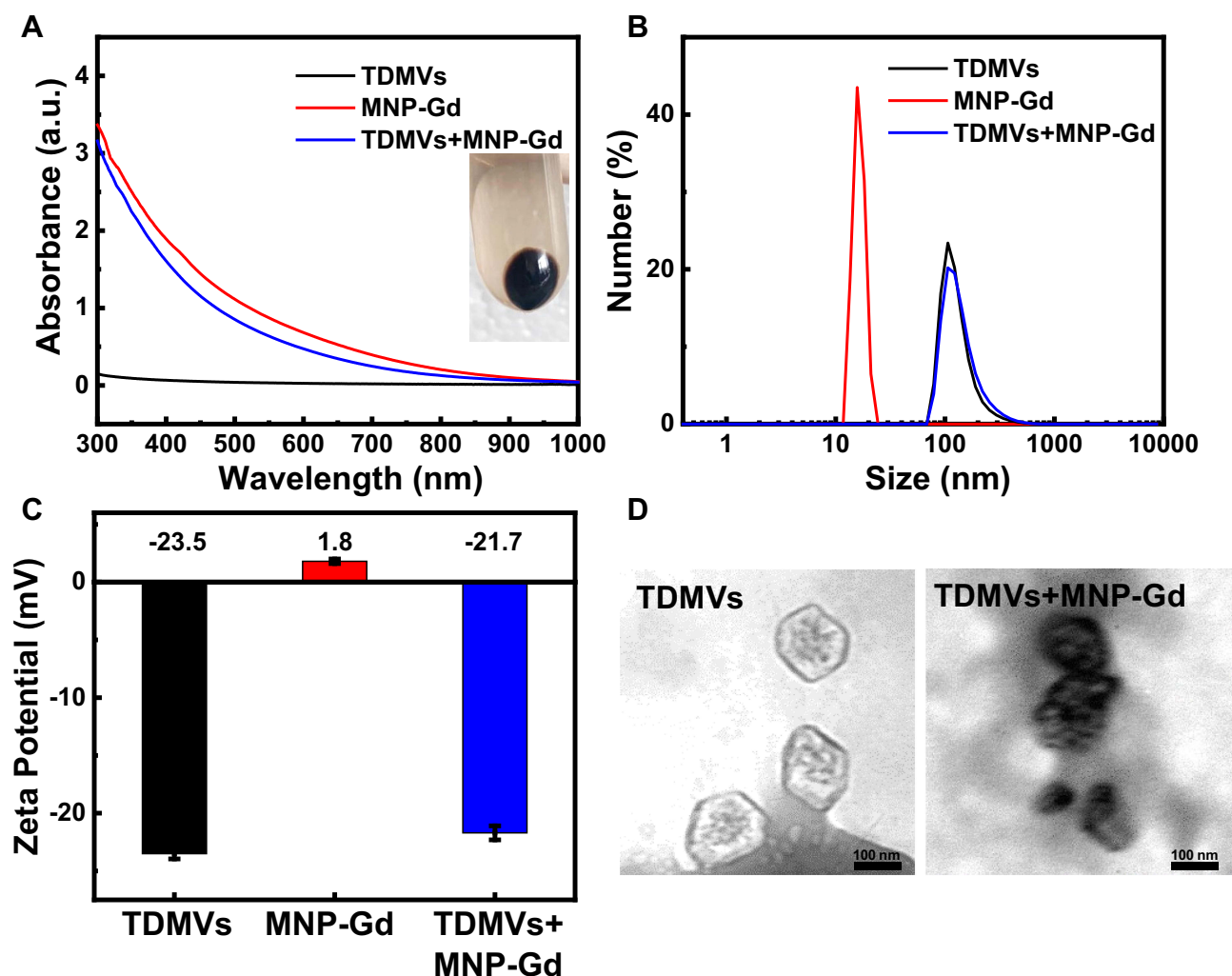
Figure 1 Characterization of TDMVs, MNP-Gd and TDMVs+MNP-Gd. (**A**) UV-vis-NIR absorption spectrum of the TDMVs, MNP-Gd and TDMVs+MNP-Gd solution. (**B**) DLS results of TDMVs, MNP-Gd and TDMVs+MNP-Gd dispersed in PBS. (**C**) Zeta potential of TDMVs, MNP-Gd and TDMVs+MNP-Gd dispersed in PBS. (**D**) TEM images of TDMVs and TDMVs+MNP-Gd.

Gd at various concentrations were shown in the inset of Figure 2A. As shown in this figure, the PAI signals exhibited a good linear relationship with the increase of TDMVs+MNP-Gd concentration from 25 to 400 μg/mL, confirming that TDMVs+MNP-Gd possessed great photoacoustic imaging capabilities. The in vitro MRI property of TDMVs+MNP-Gd was evaluated using a 3.0 T clinical MR scanner. The MR imaging capability of TDMVs+MNP-Gd in vitro was investigated by measuring T1 as a function of aqueous nanoparticles with different Gd^{3+} concentrations, which were determined using ICP-MS. The T1-weighted MRI signal gradually enhanced with the increase of Gd^{3+} concentrations (Figure 2B), revealing that TDMVs+MNP-Gd had an excellent T1-weighted MRI performance (r_1=6.192 mM^{-1}s^{-1} at 3.0 T).

Inspired by the promising results in vitro, after modification with MNP-Gd, TDMVs could be believed to be imaged in vivo with MRI and PAI. Therefore, the homing targeting ability of tumor-derived extracellular vesicles at tumor sites was assessed first. The in vivo PAI and MRI performances of TDMVs+MNP-Gd were tested in a subcutaneous H22 tumor model. As shown in Figure 3A, after injection of TDMVs+MNP-Gd through the tail vein, the intensity of PAI at the tumor site gradually enhanced over time and displayed maximum retention at 6 h post-injection. Subsequently, the PAI signal of the tumor tissue becomes slightly weakened at 8 h, and due to the metabolism of the nanoparticles, the signal continued to decay within the experimental time. Figure 3B shows the MRI images for TDMVs+MNP-Gd delivered systemically via i.v. injection over time (Figure S3). At 6 h after injection, the MRI signals reached
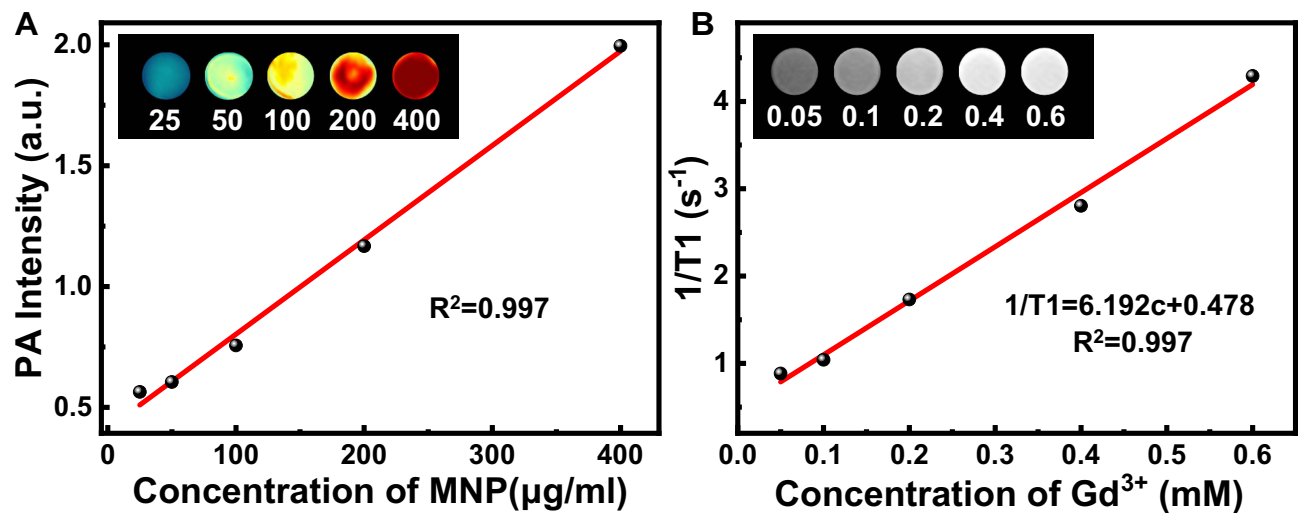
Figure 2 In vitro PA and MR imaging studies of TDMVs+MNP-Gd. (**A**) PA images of TDMVs+MNP-Gd at various concentrations (25, 50, 100, 200 and 400 μg/mL). (**B**) T1-weighted MR images and relaxivity measurements of TDMVs+MNP-Gd with different Gd^{3+} concentrations (0.05, 0.1, 0.2, 0.4 and 0.6 mM). The T1 relaxation rate as a function of Gd^{3+} concentrations.
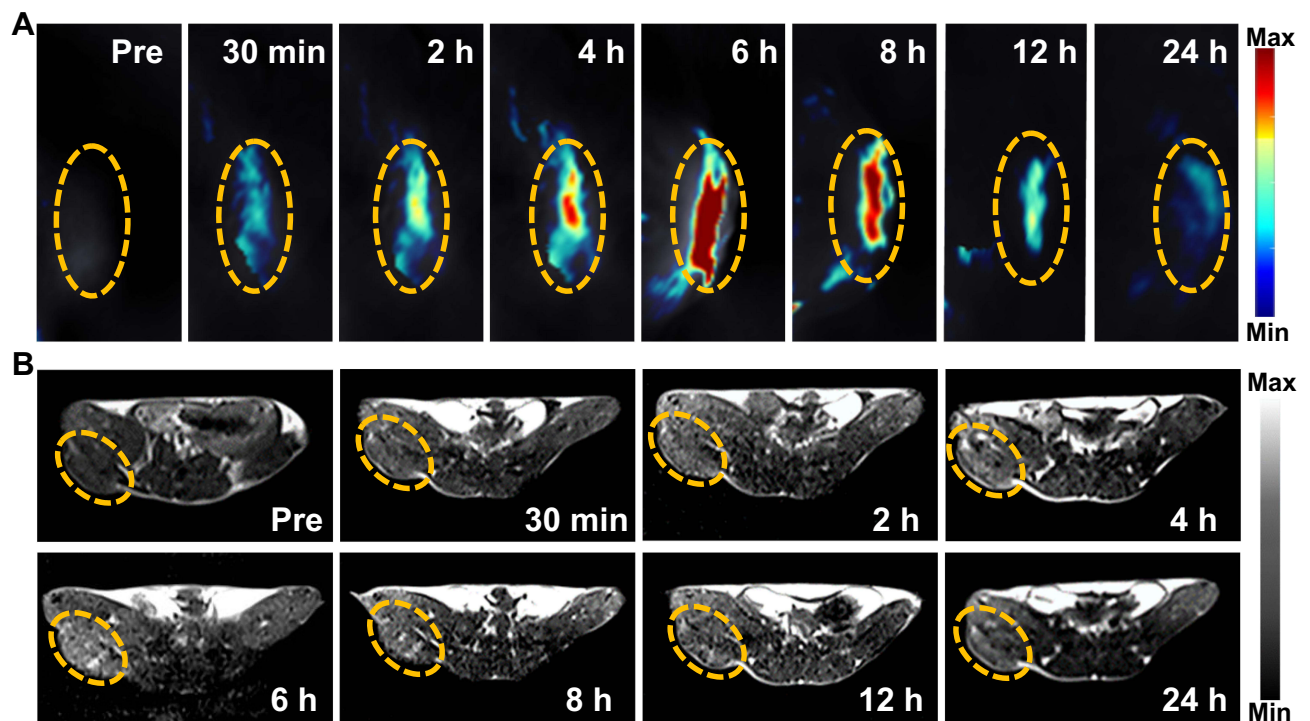

Figure 3 In vivo PA and MR imaging studies of TDMVs+MNP-Gd. (**A**) PA images in the tumor region collected by using the MOST imaging system before (pre) and at various time points after injection of TDMVs+MNP-Gd. (**B**) T1-Weighted MR axial images of tumor-bearing mice before (pre) and at various time points after injection of TDMVs+MNP-Gd using 3.0 T clinical MRI equipment. The yellow circles point to the tumor sites.

a maximum and exhibited a homogeneous distribution in the whole tumors. After that, the signal intensity of the tumor site decreased significantly over time. These in vivo imaging results at tumor sites illustrated that TDMVs had good target aggregation ability at homologous tumor sites, and the tumor aggregation behavior of TDMVs could be monitored by MNP-Gd modification.
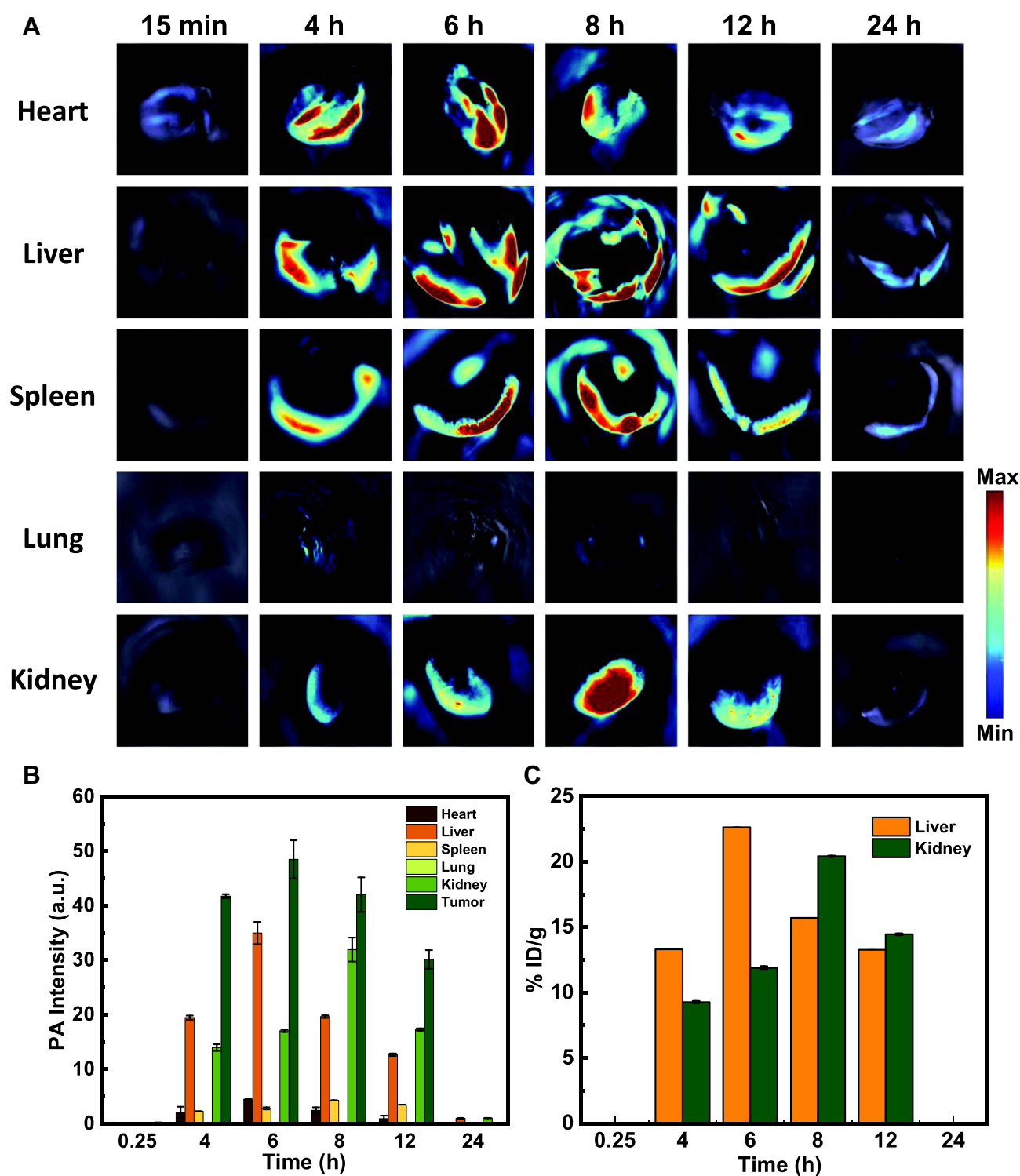
Figure 4 Biodistribution of the TDMVs+MNP-Gd. (**A**) Biodistribution of the TDMVs+MNP-Gd in main organs after i.v. injection into the tumor bearing mice using PA imaging at various time points. (**B**) PA signal intensities at various time points in tumors and the other organs. (**C**) Biodistribution of the TDMVs+MNP-Gd in liver and kidney after i.v. injection into the tumor bearing mice at various time points as determined by measuring Gd^{3+} concentrations in tissue lysates using ICP-MS.

Labeling TDMVs and visualizing their biological distribution and metabolic behavior is important for further intuitive understanding of their biological function. In addition to observing their behavior in the aggregation and distribution of tumors, the results of photoacoustic imaging of various organ tissues at different time points after tail vein injection were

analyzed for studying the biological distribution behavior of TDMVs. Over time, after 6 hours of injection, the signal intensity of the liver reached its highest level, after which it gradually decreased. However, the signal at the kidney site gradually reached its highest level after 8 hours of pre-injection. The reason for this difference in signal distribution may be that after the nanoparticles entered the body through intravenous injection, they were first taken up by the liver mononuclear phagocytosis system, then gradually metabolized in the body, and finally excreted through the kidneys (Figure 4A and B). The same results were confirmed by the Gd^{3+} amount, which was measured in the liver, kidney and other organs using ICP-MS (Figures 4C and S4).

Conclusion

TDMVs, as naturally occurring biological delivery vehicles, are of great significance in clinical applications. The development of visualization techniques for TDMVs is urgently needed to understand their biological distribution and metabolic behavior in vivo. TDMVs were modified with the help of MNP-Gd for dual-modal imaging of MRI and PAI in this work, and it was found that TDMVs could achieve good aggregation at homologous tumor sites. Additionally, after intravenous injection, TDMVs preferentially accumulated in the tumor and liver areas. Over time, the kidneys were gradually lit up, possibly related to the metabolism of TDMVs in the body. The assessment of the biodistribution behavior of TDMVs with the aid of dual-modality imaging is of great significance to address the visualization needs of extracellular vesicles. Furthermore, understanding the precise cargo transport and internalization mechanisms of TDMVs with the aid of visualization techniques is important for the successful implementations of future TDMVs derived platforms.

Funding

Disclosure

The authors report no conflicts of interest in this work.

References

1. Ratajczak J, Wysoczynski M, Hayek F, et al. Membrane-derived microvesicles: important and underappreciated mediators of cell-to-cell communication. *Leukemia*. 2006;20(9):1487–1495. doi:10.1038/sj.leu.2404296
2. EL Andaloussi S, Mager I, Breakefield XO, et al. Extracellular vesicles: biology and emerging therapeutic opportunities. *Nat Rev Drug Discov.* 2013;12(5):347–357. doi:10.1038/nrd3978
3. Van der Pol E, Boing AN, Harrison P, et al. Classification, functions, and clinical relevance of extracellular vesicles. *Pharmacol Rev.* 2012;64 (3):676–705. doi:10.1124/pr.112.005983
4. Minciacchi VR, Freeman MR, Di Vizio D. Extracellular vesicles in cancer: exosomes, microvesicles and the emerging role of large oncosomes. *Semin Cell Dev Biol*. 2015;40:41–51. doi:10.1016/j.semcdb.2015.02.010
5. Van Niel G, D'Angelo G, Raposo G. Shedding light on the cell biology of extracellular vesicles. *Nat Rev Mol Cell Biol*. 2018;19(4):213–228. doi:10.1038/nrm.2017.125
6. Théry C, Zitvogel L, Amigorena S. Exosomes: composition, biogenesis and function. *Nat Rev Immunol*. 2002;2(8):569–579. doi:10.1038/nri855
7. Armstrong JP, Stevens MM. Strategic design of extracellular vesicle drug delivery systems. *Adv Drug Deliv Rev*. 2018;130:12–16. doi:10.1016/j. addr.2018.06.017
8. Bian XJ, Xiao YT, Wu TQ, et al. Microvesicles and chemokines in tumor microenvironment: mediators of intercellular communications in tumor progression. *Mol Cancer*. 2019;18(1):50. doi:10.1186/s12943-019-0973-7
9. Piffoux M, Silva A KA, Wilhelm C, et al. Modification of extracellular vesicles by fusion with liposomes for the design of personalized biogenic drug delivery systems. *ACS Nano*. 2018;12(7):6830–6842. doi:10.1021/acsnano.8b02053
10. Sung BH, Parent CA, Weaver AM. Extracellular vesicles: critical players during cell migration. *Dev Cell*. 2021;56(13):1861–1874. doi:10.1016/j. devcel.2021.03.020
11. D'Souza-Schorey C, Clancy JW. Tumor-derived microvesicles: shedding light on novel microenvironment modulators and prospective cancer biomarkers. *Genes Dev*. 2012;26(12):1287–1299. doi:10.1101/gad.192351.112
12. Ma JW, Tang K, Zhang HF, et al. Characterization and functional analysis of tumor-derived microparticles. *Curr Protoc*. 2021;1(6):e144. doi:10.1002/cpz1.144

13. Ma JW, Zhang HF, Tang K, et al. Tumor-derived microparticles in tumor immunology and immunotherapy. *Eur J Immunol*. 2020;50 (11):1653–1662. doi:10.1002/eji.202048548

14. Tang K, Zhang Y, Zhang HF, et al. Delivery of chemotherapeutic drugs in tumour cell-derived microparticles. *Nat Commun*. 2012;3:1282. doi:10.1038/ncomms2282

15. Wan C, Sun YJ, Tian Y, et al. Irradiated tumor cell-derived microparticles mediate tumor eradication via cell killing and immune reprogramming. *Sci Adv*. 2020;6(13):eaay9789. doi:10.1126/sciadv.aay9789

16. Zhang ZJ, Xiao C, Yong TY, et al. Cellular microparticles for tumor targeting delivery: from bench to bedside. *Chem Commun*. 2020;56 (46):6171–6188. doi:10.1039/d0cc02333g

17. Zhu SL, Li SY, Yi M, et al. Roles of microvesicles in tumor progression and clinical applications. *Int J Nanomed*. 2021;16:7071–7090. doi:10.2147/IJN.S325448

18. Cheng L, Hill AF. Therapeutically harnessing extracellular vesicles. *Nat Rev Drug Discov*. 2022;21(5):379–399. doi:10.1038/s41573-022-00410-w

19. Gangadaran P, Hong CM, Ahn BC. Current perspectives on in vivo noninvasive tracking of extracellular vesicles with molecular imaging.. *Biomed Res Int*. 2017;2017:9158319. doi:10.1155/2017/9158319

20. Wang DD, Yao YZ, He JK, et al. Engineered cell-derived microparticles Bi$_2$Se$_3$/DOX@MPs for imaging guided synergistic photothermal/low-dose chemotherapy of cancer. *Adv Sci*. 2020;7(3):1901293. doi:10.1002/advs.201901293

21. Yu ZL, Zhang W, Zhao JY, et al. Development of a dual-modally traceable nanoplatform for cancer theranostics using natural circulating cell-derived microparticles in oral cancer patients. *Adv Funct Mater*. 2017;27(40):1703482. doi:10.1002/adfm.201703482

22. Chuo ST, Chien JC, Lai CP. Imaging extracellular vesicles: current and emerging methods. *J Biomed Sci*. 2018;25(1):91. doi:10.1186/s12929-018-0494-5

23. Gangadaran P, Hong CM, Ahn BC. An update on in vivo imaging of extracellular vesicles as drug delivery vehicles. *Front Pharmacol*. 2018;9:169. doi:10.3389/fphar.2018.00169

24. Zhao JY, Chen G, Gu YP, et al. Ultrasmall magnetically engineered Ag$_2$Se quantum dots for instant efficient labeling and whole-body high-resolution multimodal real-time tracking of cell-derived microvesicles. *J Am Chem Soc*. 2016;138(6):1893–1903. doi:10.1021/jacs.5b10340

25. Cai Z, Fu Y, Qiu Z, et al. Multitarget reaction programmable automatic diagnosis and treatment logic device. *ACS Nano*. 2021;15 (12):19150–19164. doi:10.1021/acsnano.1c07307

26. Caspani S, Magalhaes R, Araujo JP, et al. Magnetic nanomaterials as contrast agents for MRI. *Materials*. 2020;13(11):2586. doi:10.3390/ma13112586

27. Zhang X, Ong'achwa Machuki J, Pan WZ, et al. Carbon nitride hollow theranostic nanoregulators executing laser-activatable water splitting for enhanced ultrasound/fluorescence imaging and cooperative phototherapy. *ACS Nano*. 2020;14(4):4045–4060. doi:10.1021/acsnano.9b08737

28. Morse SV, Boltersdorf T, Harriss BI, et al. Neuron labeling with rhodamine-conjugated Gd-based MRI contrast agents delivered to the brain via focused ultrasound. *Theranostics*. 2020;10(6):2659–2674. doi:10.7150/thno.42665

29. Fatima A, Ahmad MW, Al Saidi KA, et al. Recent advances in gadolinium based contrast agents for bioimaging applications. *Nanomaterials*. 2021;11(9):2449. doi:10.3390/nano11092449

30. Sun JH, Xu W, Li LP, et al. Ultrasmall endogenous biopolymer nanoparticles for magnetic resonance/photoacoustic dual-modal imaging-guided photothermal therapy. *Nanoscale*. 2018;10(22):10584–10595. doi:10.1039/c8nr01215f

31. Zhang X, Xi ZQ, Ong'achwa Machuki J, et al. Gold cube-in-cube based oxygen nanogenerator: a theranostic nanoplatform for modulating tumor microenvironment for precise chemo-phototherapy and multimodal imaging. *ACS Nano*. 2019;13(5):5306–5325. doi:10.1021/acsnano.8b09786

32. Fan QL, Cheng K, Hu X, et al. Transferring biomarker into molecular probe: melanin nanoparticle as a naturally active platform for multimodality imaging. *J Am Chem Soc*. 2014;136(43):15185–15194. doi:10.1021/ja505412p

33. Hong ZY, Feng HY, Bu LH. Melanin-based nanomaterials: the promising nanoplatforms for cancer diagnosis and therapy. *Nanomedicine*. 2020;28:102211. doi:10.1016/j.nano.2020.102211

34. Lemaster JE, Wang Z, Hariri A, et al. Gadolinium doping enhances the photoacoustic signal of synthetic melanin nanoparticles: a dual modality contrast agent for stem cell imaging. *Chem Mater*. 2019;31(1):251–259. doi:10.1021/acs.chemmater.8b04333

35. Liu JJ, Wang Z, Nie LM, et al. RGD-functionalised melanin nanoparticles for intraoperative photoacoustic imaging-guided breast cancer surgery. *Eur J Nucl Med Mol Imaging*. 2022;49(3):847–860. doi:10.1007/s00259-021-05545-3

36. Sun JH, Cai WW, Sun Y, et al. Facile synthesis of melanin-dye nanoagent for NIR-II fluorescence/photoacoustic imaging-guided photothermal therapy. *Int J Nanomed*. 2020;15:10199–10213. doi:10.2147/IJN.S284520

37. Zhang L, Sheng D, Wang D, et al. Bioinspired multifunctional melanin-based nanoliposome for photoacoustic/magnetic resonance imaging-guided efficient photothermal ablation of cancer. *Theranostics*. 2018;8(6):1591–1606. doi:10.7150/thno.22430

38. Zhang RP, Fan QL, Yang M, et al. Engineering melanin nanoparticles as an efficient drug-delivery system for imaging-guided chemotherapy. *Adv Mater*. 2015;27(34):5063–5069. doi:10.1002/adma.201502201

39. Wang WD, Chen C, Ying Y, et al. Smart PdH@MnO$_2$ yolk–shell nanostructures for spatiotemporally synchronous targeted hydrogen delivery and oxygen-elevated phototherapy of melanoma. *ACS Nano*. 2022;16(4):5597–5614. doi:10.1021/acsnano.1c10450

40. Sun JH, Li XY, Chen AQ, et al. A dual-modality MR/PA imaging contrast agent based on ultrasmall biopolymer nanoparticles for orthotopic hepatocellular carcinoma imaging. *Int J Nanomed*. 2019;14:9893–9904. doi:10.2147/IJN.S219794